HHS Public Access

Author manuscript

Otol Neurotol. Author manuscript; available in PMC 2019 August 01.

Published in final edited form as:

Otol Neurotol. 2018 August ; 39(7): 922–928. doi:10.1097/MAO.0000000000001850.

Preliminary results with image-guided cochlear implant insertion techniques

Robert F. Labadie, M.D., Ph.D. and
Dept. of Otolaryngology – Head and Neck Surgery, Vanderbilt University Medical Center

Jack H. Noble, Ph.D.
Dept. of Electrical Engineering & Computer Science, Vanderbilt University

Abstract

Hypothesis: Using patient-customized cochlear measurements obtained from pre-operative CT scans to guide insertion of cochlear implant (CI) electrode arrays will lead to more optimal intracochlear positioning.

Background: Cochlear duct length is highly variable ranging from 25.26–35.46mm (Hardy, 1938), yet CI electrode arrays are treated as one size fits most. We sought to investigate the impact of patient-customized insertion plans on final location of electrode arrays.

Methods: Twenty cadaveric temporal bone specimens were CT scanned and randomly divided into groups A and B. Group A specimens had an optimal customized insertion plan generated including entry site (e.g. round window (RW) versus extended RW), entry vector based on anatomical landmarks (e.g. hug posterior aspect of facial recess and angle 1mm inferior to stapes), depth to begin advancing off stylet, and final insertion depth. Suboptimal plans were chosen for group B by selecting an approach that was normal yet predicted to result in poor final electrode location. One surgeon, blinded as to group, carried out the CI insertions following which the electrode array was fixed using superglue and the specimen CT scanned to allow assessment of final electrode location.

Results: Average perimodiolar distance for groups A and B were 0.51 and 0.60 mm, respectively. For group A, full scala tympani insertion was achieved in all specimens while in group B, four of ten specimens had scalar translocation.

Conclusions: Patient customized cochlear implant insertion techniques achieved better positioning of electrode arrays in this study and have potential for improving electrode positioning in patients.

Keywords

cochlear implants; image-guidance; insertion techniques

Please send correspondence to: Prof. Jack H. Noble, Dept. of EECS, Vanderbilt University, 2301 Vanderbilt Pl., Box 1679 Station B, Nashville, TN 37235, Phone: 615-875-5539, Fax: 615-343-5459, jack.noble@vanderbilt.edu.

Disclosures: Dr. Labadie is a consultant for Advanced Bionics and Ototronix.

Introduction

Cochlear implants (CIs) are surgically implanted neural prosthetic devices used to treat severe-to-profound hearing loss. With well over 324,000 recipients worldwide, CIs are considered standard of care treatment for severe-to-profound sensorineural hearing loss [1]. CIs restore hearing by applying electric potential to neural stimulation sites in the cochlea with a surgically implanted electrode array (EA). Implants available today produce remarkable results for the vast majority of recipients with average postoperative word and sentence recognition approximating 60% and 70% correct, respectively, for unilaterally implanted recipients and 70% and 80% correct for bilateral recipients [2–6]. Despite this success, a significant number of users receive marginal benefit, and restoration to normal fidelity is rare even among the best performers.

Cochlear implant EAs can be broadly divided into straight and pre-curved models. Straight arrays are intended to follow and rest against the outer wall of scala tympani (ST). In contrast, pre-curved arrays are designed such that their resting state curvature roughly approximates that of an average human cochlea facilitating perimodiolar positioning, i.e., positioning the electrodes close to the inner (modiolar) wall of ST. In practice, a pre-curved array is loaded onto a straightening stylet which is inserted into the basal turn following which it is advanced off the stylet (AOS) and resumes its coiled shape as it navigates the cochlear turns. Perimodiolar positioning is desired because it both (i) uses less energy for stimulation and (ii) results in better spectral resolution and potentially patient outcomes by providing more discrete stimulation with less interference from neighboring electrodes [7]. However, because the interior of the cochlea is invisible to the surgeon, the intra-cochlear path of the array and final positioning (perimodiolar versus lateral placement) of the EA are generally unknown.

Research by multiple groups has shown that atraumatic, perimodiolar placement of precurved EAs within ST maximizes post-implantation hearing outcomes [7–9]. However, pre-curved EAs have a high rate of translocation (Wanna et al. [10] report 42%) and are typically not perimodiolar [11]. Despite overwhelming evidence that sub-optimal EA placement is linked with poorer outcomes and that intracochlear anatomical variability is substantial [12–13], technical innovations introduced by CI companies have focused on generic, one-size-fits-most EA design rather than customized insertion techniques based on patient specific anatomy. A notable exception is the variable length straight electrodes (24, 28, and 31mm) available from one manufacturer (Medel, Innsbruck, Austria). In selecting which length to use, measurement of the cochlear duct is performed on preoperative CT scans [14]. However, this approach requires expertise in reorienting and measuring CT scans and has recently been shown to have low repeatability [15] and, to date, no impact on final hearing outcomes.

A major issue that has limited advancement in this area is difficulty in accurately measuring cochlear anatomy because intracochlear structures approach the typical resolution of clinical CTs. To overcome this limitation, research by our group has led to the development of automated image analysis algorithms that rely on a high-resolution micro-CT (μCT) atlas of cadaveric cochlear anatomy to predict patient-specific cochlear anatomy in a clinical CT

image with a high degree of accuracy [16–17]. Because these techniques are accurate and completely automated, they remove both the technical and clinical barriers for patient-specific analyses of the cochlea and enable development of patient-customized CI electrode placement procedures. In this work, we present preliminary results from a blinded, randomized temporal bone study comparing final EA position for cochleae implanted with customized optimal insertion plans versus suboptimal insertion plans.

Methods

In this work, we hypothesize that analysis of temporal bone anatomy, i.e., the shape of ST and SV, in the pre-operative CT image can be used to recommend an approach vector, array base insertion depth, and AOS depth and orientation for pre-curved EAs. To segment ST and SV, we use a non-rigid statistical shape model [18] created with μCT images of 9 cochleae specimens in which intra-cochlear structures are visible [16–17]. These models are then automatically fit to the external boundary of the patient cochlea that is visible in conventional CT allowing highly accurate estimation of the position of internal cochlear structures not visible in the CT. Figure 1a–c shows a portion of a pre-operative CT scan and the results obtained with our segmentations presented as 3D surfaces and 2D contours.

To make recommendations for the insertion procedure, we expand upon a technique proposed to estimate the optimal final position of the array for a patient based on their cochlear shape [11]. First, an EA shape model is created. While our methods could apply to any pre-curved array, in this work we chose to use the Advance Bionics Mid-Scala (MS) array due to the availability of practice arrays for use in this study. The model is created by acquiring a CT image of the EA in air under no load and measuring the 3D position of each electrode in the array in the image. This provides an estimation of the resting state shape of the array. Next, to define the ideal modiolar position of the array for a new patient, the ideal modiolar position of ST is localized in our statistical shape model that we use to localize intra-cochlear anatomy. This was done by manually defining a 3D modiolar hugging curve as a sequence of points within the ST using 3D object editing software developed in-house. This manually defined modiolar hugging curve is automatically transformed to each patient's pre-implant CT using a Thin Plate Spline registration [20] of the model ST surface to the patient's ST surface. The result of this process is shown as the blue curve in Figure 1d. Finally, the EA shape model is rigidly registered to the patient's modiolar curve using an iterative closest point registration technique [21] which places the resting state shape of the EA within the patient's ST such that the EA best matches the patient's modiolar curve as shown in Figure 1 (d), which depicts the EA shape model (green) after registration to the modiolar curve (blue). This registered EA shape model is used to determine patient-customized insertion plans specifying (i) overall insertion depth, (ii) AOS insertion depth, and (iii) trajectory orientation as described below.

To determine overall insertion depth, we use the technique described by Wang et al. [11] to specify where the base marker should be placed relative to the entry into the cochlea (e.g. in Figure 1d, the depth is specified as 2mm outside of the cochlea). To determine the depth at which AOS is to begin, we combine the resting state shape of the array with the stylet position-dependent trajectory model proposed by McBrayer et al. [23]. To do this, a group of

9 practice MS arrays underwent AOS deployment in increments of approximately 2mm (exact distance of stylet withdrawn was measured precisely using digital calipers under a microscope) with 3D reconstruction at each interval of deployment facilitated by CT scanning. Three interval results of this process are shown in Figure 3, superimposed onto a patient's cochlea. The last panel corresponds to the shape of the array with the stylet fully withdrawn (i.e. the resting state shape). Using these 9 exemplars, we can simulate the shape of the array at any AOS distance by interpolating a weighted average between shapes. For interpolation we treat each EA as a sequence of linear segments attached at joints corresponding to each electrode. To predict interval shapes comprising the trajectory of an EA electrode undergoing AOS, we linearly interpolate the joint angles between exemplar arrays. Applying this model to the generically recommended AOS depth, agreement between the EA trajectory and the modiolar curve was found to average approximately 0.5mm [23]. To determine each patient-customized AOS depth, this model was aligned with the individualized cochlear anatomy with AOS depth chosen as that which resulted in the best agreement between the model and modiolar curve (see Figure 1d). Finally, recommended orientation is chosen as the orientation of the aligned model, which matches the orientation of the basal turn of the ST.

Choosing the best entry vector and site is done by determining a trajectory that is as close as possible to being collinear with the basal turn of the ST while also passing through the facial recess and either an extended round window cochleostomy, or, preferably, directly through the round window. An example of an optimal array entry vector (yellow cylinder) with the structures of interest, which are automatically segmented in pre-operative CT using previously published techniques [29,30], is shown in Figure 1e. In this case, the optimal entry vector that is collinear with the base of the ST passes directly adjacent to the facial nerve through an extended RW entry site of the ST, thus this would be the recommended entry vector and site for this case.

We evaluated our approach using a set of 20 temporal bone specimens. Each specimen underwent CT scanning using clinically applicable protocols. After performing a mastoidectomy and posterior tympanotomy, each specimen was implanted by an experienced surgeon. The specimens were randomly divided into two groups (*A* and *B*). For each specimen in group *A*, using the pre-operative CT scan, an optimized plan was generated as proposed above. Group *B* served as the control group with a realistic plan but predicted by our process to lead to poor electrode placement. The surgeon was blinded regarding which group an individual specimen was randomized into.

A quantitative summary of the instructions for each case are included as Supplementary Table 1. For each case in the table, shown are whether it belongs to the proposed method (*A*) or control (*B*) group, the angle between the orientation of the basal turn and the proposed entry trajectory in both superior-inferior (S-I) and anterior-posterior (A-P) directions, and the orientation of the electrodes relative to orientation of the basal turn. These angular measurements are visualized in Figure 1e. Also shown in Supplementary Table 1 are the recommended entry approach of either round window (RW) or extended round window (ERW), the recommended depth to initial AOS relative to the generically recommended AOS depth, and the recommended overall insertion depth relative to the generically

recommended insertion depth. To show how different the control plan AOS and insertion depths are from what the plan using the proposed approach would be for these cases, also shown for the control cases are the optimal AOS and overall depth of insertions determined by our proposed techniques. For cases 1–10, we had not yet implemented the image-guided recommendation for the electrode orientation relative to the basal turn orientation, and thus this column is empty. Visualizations of the EA model projected onto the ST for a control case (#12) are shown in Figure 3. As can be seen in the figure, for this case using the electrode trajectory model, a good AOS depth and sub-optimal overall depth were chosen for the control plan. Further, as shown in Supplementary Table 1, the entry vector was deviated from the optimal approach in this case. Group *B* plans such as this one were designed such that they disagree with the optimized plan in one or more quantities, but have an entry vector that falls within the range of typical entry vectors and have insertions depths that vary closely around the generically recommended depths.

The surgeon was presented the insertion plan in textual format. For the sake of simplicity and so that it was feasible for the surgeon to implement the plan, we converted the specific insertion vector angle quantities and electrode insertion depths into relatively coarse instructions related to reference structures that could be directly visualized. For example, one plan (case 12) was:

> *Entry site*: Insert through the RW membrane.
>
> *Entry vector*: Choose entry angle to pass through the middle of the facial recess. Face electrodes between the stapes footplate and IS-joint.
>
> *AOS depth*: Insert array on stylet until the AOS marker is 1.5 mm inside the round window and electrode 7 is even with the RW.
>
> *Base insertion depth*: Advance off the static stylet until proximal insertion depth marker reaches the round window.

The instructions for all cases were selected such that they were coarse enough that they were easy to implement. For example, the posterior-anterior angle of the entry vector could hug the anterior wall, posterior wall, or pass through the middle of the facial recess, and the superior-inferior angle of the entry vector could either pass 1 mm inferior to the stapes, through the middle of the facial recess, or hug the inferior portion of the facial recess. After implantation, a post-implantation CT was acquired to evaluate electrode position using automated techniques that have been previously developed [24–25]. Outcome measures included scalar location, modiolar distance, angular insertion depth, and base insertion depth.

In addition to the temporal bone dataset, with IRB approval we also used our image analysis techniques to retrospectively determine the same electrode position outcome measures in CT images from a group of 17 patients who have been implanted with MS arrays at our center. Outcomes measured in this dataset serve as a clinical baseline to be compared to outcomes in our *A* and *B* groups.

Results

The image processing computations for each case required approximately 2 minutes to execute on a standard PC. The results for each individual case in our study are shown in Table 1. In the table, shown are the group, resulting scalar location ("ST" for full ST placement versus "ST-SV" for arrays that translocate from ST into SV), angular depth of insertion in degrees, the average distance of the electrodes to the modiolus (Mean Modiolar Dist), and the overall depth of insertion measured as the signed distance between the depth marker and the round window, with negative distances indicating extracochlear placement of the depth marker. Electrode position was measured using automated techniques [24–25] in postoperative CT scans and confirmed visually using high resolution μCTs for each specimen. Optimal outcome would be scalar location within the ST with high angular depth of insertion, small modiolar distance, and good agreement between the actual and planned overall insertion depth. Overall statistics are shown in Table 2. Also shown in the table are the results from the group of 17 actual patients (Pat) who have been implanted with MS arrays at our center. Two-tailed rank sum tests were used to assess statistical differences in the rate of scalar location among the different groups. Unpaired two-tailed t-tests were used to assess statistical differences in angular depth, modiolar distance, and agreement between the actual and planned insertion depth of the base of the array. As shown in Table 2, no statistically significant differences were detected between the control and patient groups, implying that our control test instructions and results were not dissimilar to traditional surgical techniques.

Our patient-customized insertion plans, Group *A*, resulted in full ST placement in every case, which was a statistically significantly higher rate of full ST placement than the control tests, Group *B*, and the patient cases. Statistically significant differences were not detected in angular insertion depth nor in the difference between the actual and the planned base insertion depth. Thus, adherence to the planned base insertion depth was good. The exception is case 17, where under-insertion occurred. This was the only case resulting in extra-cochlear electrodes (E15-E16). It is unknown whether this array was under-inserted initially or backed out after the insertion procedure due to suboptimal fixation. Overall mean modiolar distance was reduced with group *A* plans, but this difference was not found to be statistically significant in this relatively small study with N=10 samples in each *A* and *B* group. Based on our current dataset, we estimate an N=24 study would provide power of 0.8 to detect a significant difference.

To show differences on an electrode-by-electrode basis, Figure 4 depicts the average modiolar distance for each of the 16 electrodes at their average angular insertion depth for the control, Group B, (red) and patient-customized, Group A, (green) cases. The vertical lines in the figure represent the standard deviation of the modiolar distance for each electrode. This plot shows that on average across the control experiments, the middle portion of the array is lifted away from the modiolus, even though the insertion depth marker was not advanced past the round window for any case. The group *A* plans are more perimodiolar for the middle and apical portions of the array while sacrificing some modiolar proximity at the base of the array. Two sample, two-tailed t-tests with unequal variance were performed for each electrode individually across the *A* and *B* groups. After Bonferroni correction for

multiple comparisons, it was found that the group *A* plans resulted in significantly lower modiolar distance for E6–E9 and significantly higher distance for E15-E16. This can be visually appreciated in three-dimensional renderings of representative group *A* and *B* cases shown in Figure 2. As can be seen in the figure, the middle portion of the array in the control case 3 (a, b) lifts away from the modiolus, whereas the array in the group *A* case 18 (c, d) is perimodiolar.

General linear models were used to detect which guidance quantities, if any, were significantly associated with the final scalar location, angular depth, and mean modiolar distances. We found scalar translocation to be significantly associated with disagreement between the planned and optimal basal turn trajectory superior-inferior angle (r=0.83; p=6e-4). Mean modiolar distance was associated with differences between optimal and planned base insertion depth, entry point, and basal turn trajectory superior-inferior angle (r=0.77; p=2e-3). Overall angular depth was associated with differences between planned and optimal entry point and basal turn trajectory anterior-posterior angle (r=0.72; p=2e-3).

Discussion

Health care is rapidly entering the era of personalized medicine, also known as precision medicine, in which treatment modalities are tailored to individual patient attributes. First applied to pharmacogenetics (i.e. selecting drugs based on genetic traits), it is also true for devices particularly with skeletal implants (e.g. craniofacial reconstructions, joint replacements). Within the field of cochlear implantation, we have yet to enter this new era and continue to use universal sized electrodes to fit all cochlea despite evidence that the cochlea exhibits large inter-patient variability (Hardy, 1938). The excellent average postoperative word and sentence recognition scores of approximately 60% and 70% correct, respectively, achieved with the standard-of-care approach are widely attributable to the plasticity of the central nervous system adapting to the electrical input, yet better matching of CI EA's to the anatomy via a personalized approach has promise of leading to even better potential performance.

For this first implementation of a patient-customized, image-guided insertion plan, we developed a strategy for conveying insertion plans without the use of intra-operative tracking in an effort to facilitate clinical adoption. All of the surgical technique recommendations were provided to the surgeon in the form of textual instructions that referenced anatomical landmarks. Our initial findings (Table 1) indicate that the implanting surgeon could follow these instructions well routinely achieving excellent matching of the proposed insertion depth with the measured insertion depth (range 0–1.5mm, average=0.7mm, median =1.1mm, mode=0mm) excluding an outlier of 2.9 mm thought to have occurred secondary to migration before adequate fixation.

Our findings confirm that generic insertion plans tend to lead to over-insertion accompanied by buckling of the EA away from the modiolus and against the lateral wall. Once the base of the array has been inserted to the recommended depth, it is likely that the array has returned to its resting shape and the tip of the array has reached the desired angular insertion depth with any further insertion not leading to further advancement of the tip. A clinical example

case where this has likely occurred is shown in Figure 2a where the basal depth marker was inserted ~2mm past the recommended depth. Advancement of the base of the array beyond the recommend depth resulted in the lateral displacement of the EA away from the modiolar wall in the mid region. On the other hand, inserting the base of the array shallower than the recommended depth may lead to shallower depth of the tip of the array, which also could be detrimental to outcome as the range of nerves stimulated may be reduced.

A potential drawback of our approach which tends to recommend shallower insertion depths is that the most basal electrodes (e.g., E15, E16) are more distant from the modiolus (Figure 4). However, these electrodes could be deactivated with recent research studies supporting improvement in outcomes with deactivation of suboptimally positioned electrodes [26–28]. We hypothesize that the benefits of better perimodiolar positioning of the rest of the array will outweigh this potential drawback.

One limitation of our approach as it was initially implemented is that it references a surgically created space, the facial recess, whose shape cannot be precisely predicted from pre-operative CT scans. We used relatively coarse instructions (e.g., hug the posterior wall, the anterior wall, or remain in the mid region of the facial recess) but found that such instructions correlated with final electrode positioning as assessed by general linear modeling. To further explore this, in future work we will evaluate how well the surgically implemented vector agrees with the planned one using optically tracked insertion tools. Another limitation is the use of a single EA. In future studies, we plan to evaluate our techniques with additional EAs including the Contour Advance (CA) and 532 (Cochlear Corporation; Sydney, Australia). Towards this end, we have already created an array trajectory model for the CA similar to the one used in this study for the MS. In Supplementary Figure 1, we have registered the MS and CA models and found the resting-state shape of the two to be quite similar. We also have performed retrospective analysis the CA and MS EA's using post-operative CT scans of CI patients in our imaging database and have found positioning of the two arrays to be quite similar (MS: average insertion depth = 393°, average modiolar distance = 0.54mm (N=17); CA: average insertion depth = 377°, average modiolar distance = 0.48 mm (N=79)). Thus, we anticipate that the methods we have evaluated in this study will lead to similar results with CA arrays. Yet another limitation is that our patient-customized, image-guided insertion plan are only applicable for cochleae free of anatomical malformations. And, while pre-curved arrays were the focus of this work, our techniques could also be applied to straight EAs with slightly different strategies necessary to recommend overall insertion depth and angle of insertion.

Conclusions

In this work, we have proposed and implemented a simple, image-guided approach for patient-customized CI electrode insertion. Preliminary results indicate that this method results in significantly higher rates of ST placement and better perimodiolar positioning of the middle section of the EA. We plan to confirm these exciting preliminary findings in a larger study and explore the potential impact on hearing outcomes.

Supplementary Material

Refer to Web version on PubMed Central for supplementary material.

Acknowledgements:

This work was supported by grant R01008408 from the National Institute on Deafness and other Communication Disorders. The content is the sole responsibility of the authors and does not necessarily reflect the views of this institute. The authors would also like to thank Advanced Bionics for providing materials used in this study.

References

[1]. National Institute on Deafness and Other Communication Disorders, “Cochlear Implants,” No. 11–4798, 2014.

[2]. Buss E, Pillsbury HC, Buchman CA, Pillsbury CH, Clark MS, Haynes DS, Labadie RF, Amberg S, Roland PS, Kruger P, Novak MA, Wirth JA, Black JM, Peters R, Lake J, Wackym PA, Firszt JB, Wilson BS, Lawson DT, Schatzer R, DHP S, Barco AL: Multicenter U.S. Bilateral med-el cochlear implantation study: Speech perception over the first year of use. Ear Hear 2008;29:20–32. [PubMed: 18091099]

[3]. Dorman MF, Yost W, Wilson BS, Gifford RH: Speech perception and sound localization by adults with bilateral cochlear implants. Seminars in Hearing 2009;32:73–89.

[4]. Gifford RH, Shallop JK, Peterson AM. (2008). Speech Recognition Materials and Ceiling Effects: Considerations for Cochlear Implant Programs. Audiol Neurotol, 13:193–205.

[5]. Gifford RH, Dorman MF, Sheffield SW, Teece K, Olund AP. “Availability of binaural cues for bilateral cochlear implant recipients and bimodal listeners with and without hearing preservation.” Audiol Neurotol. 2014;19(1):57–71

[6]. Litovsky RY, Parkinson A, Arcaroli J, Sammeth C: Simultaneous bilateral cochlear implantation in adults: A multicenter clinical study. Ear Hear 2006;27:714–730. [PubMed: 17086081]

[7]. Holden LK, Finley CC, Firszt JB, Holden TA, Brenner C, Potts LG, Gotter BD, Vanderhoof SS, Mispagel K, Heydebrand G, Skinner MW., “Factors affecting open-set word recognition in adults with cochlear implants,” Ear Hear. 34(3):342–60, 2013. [PubMed: 23348845]

[8]. Carlson ML, Driscoll CL, Gifford RH, Service GJ, Tombers NM, Hughes-Borst BJ, Neff BA, Beatty CW. Implications of minimizing trauma during conventional cochlear implantation. Otol Neurotol. 32(6):962–8, 2011. [PubMed: 21659922]

[9]. Wanna GB, Noble JH, Gifford RH, Dietrich MS, Sweeney AD, Zhang D, Dawant BM, Rivas A, Labadie RF. “Impact of Intrascalar Electrode Location, Electrode Type, and Angular Insertion Depth on Residual Hearing in Cochlear Implant Patients: Preliminary Results.” Otol Neurotol. 36(8):1343–8, 2015. [PubMed: 26176556]

[10]. Wanna GB, Noble JH, Carlson ML, Gifford RH, Dietrich MS, Haynes DS Dawant BM, and Labadie RF, “Impact of Electrode Design and Surgical Approach on Scalar Location and Cochlear Implant Outcomes,” Laryngoscope, vol. 124(S6), pp. S1–7, 2014.

[11]. Wang J, Dawant BM, Labadie RF, Noble JH, “Retrospective evaluation of a technique for patient-customized placement of pre-curved cochlear implant electrode arrays,” Otolaryngology – Head and Neck Surgery, 2016 (in press)

[12]. Hardy M “The Length of the Organ of Corti in Man,” American Journal of Anatomy, 62(2), 1938, p. 179–311.

[13]. Pelosi S and Noble J (co-first authors), Dawant B, and Labadie RF. “Analysis of inter-subject variations in promontory and intracochlear anatomy for cochlear implantation,” Otology and Neurotology vol. 34(9), pp. 1675–1680, 2013. [PubMed: 24232065]

[14]. Escudé B, James C, Deguine O, Cochard N, Eter E, Fraysse B. The size of the cochlea and predictions of insertion depth angles for cochlear implant electrodes. Audiol Neurotol. 2006;11 Suppl 1:27–33.

[15]. Rivas A, Cakir A (co-first authors), Hunter J, Labadie RF, Zuniga GM, Wanna GB, Dawant BM, Noble JH, “Automatic cochlear duct length estimation for selection of cochlear implant electrode arrays,” Otology & Neurotology vol. 38(3), pp. 339–346, 2017. [PubMed: 28146009]

[16]. Noble JH, Labadie RF, Majdani O and Dawant BM, “Automatic segmentation of intra-cochlear anatomy in conventional CT”, IEEE Trans. Biomedical. Eng, vol. 58, no. 9, pp.2625–2632, 2011.

[17]. Noble JH, Gifford RH, Labadie RF, Dawant BM, 2012, “Statistical Shape Model Segmentation and Frequency Mapping of Cochlear Implant Stimulation Targets in CT,” Ayache N et al. (Eds.): MICCAI 2012, Part II, LNCS 7511, pp. 421–428. 2012.

[18]. Cootes TF, Taylor CJ, Cooper DH, Graham J, “Active Shape Models-Their Training and Application,” Computer Vision and Image Understanding 61(1), pp. 38–59, 1995.

[19]. Press WH, Flannery BP, Teukolsky SA, et al. Numerical Recipes in C. 2nd ed Cambridge, UK: Cambridge University Press; 1992:412–419.

[20]. Goshtasgy A Registration of images with geometric distortions. IEEE Tran Geosci Remote Sens. 1988;26:60–64.

[21]. Besl PJ, McKay ND. A method for registration of 3-D shapes. IEEE Trans Pattern Anal Mach Intell. 1992;14:239–256.

[22]. Schonemann PH, “A generalized solution of the orthogonal Procrustes problem,” Psychometrika, vol. 31, pp. 1–10, 1966.

[23]. McBrayer K, Wanna GB, Labadie RF, Dawant BM, Noble JH, “Analysis of patient-specific variability in optimal cochlear implant insertion depths,” Oral presentation at the American Neurotology Society, 2015.

[24]. Zhao Y, Dawant BM, Labadie RF, and Noble JH, “Automatic Localization of Cochlear Implant Electrodes in CT,” Lecture Notes in Computer Science-Proceedings of MICCAI, vol. 8673, pp. 331–8, 2014.

[25]. Noble JH and Dawant BM, “Automatic graph-based localization of cochlear implant electrodes in CT,” Lecture Notes in Computer Science-Proceedings of MICCAI, vol. 9350, pp. 152–9, 2015.

[26]. Noble JH, Labadie RF, Gifford RH, Dawant BM, “Image-guidance enables new methods for customizing cochlear implant stimulation strategies,” IEEE Trans Neural Syst Rehabil Eng. vol. 21(5):820–9, 2013. [PubMed: 23529109]

[27]. Noble JH, Gifford RH, Hedley-Williams AJ, Dawant BM, and, Labadie RF, “Clinical evaluation of an image-guided cochlear implant programming strategy,” Audiology & Neurotology, vol. 19, pp. 400–11, 2014. [PubMed: 25402603]

[28]. Noble JH, Hedley-Williams AJ, Sunderhaus LW, Dawant BM, Labadie RF, Camarata SM, Gifford RH, “Initial results with image-guided cochlear implant programming in children,” Otology & Neurotology 37(2), pp. 69–9, 2016.

[29]. Noble JH, Dawant BM, Warren FM, Labadie RF, “Automatic Identification and 3D Rendering of Temporal Bone Anatomy,” Otol & Neurotol, 30(4):436–42, 2009.

[30]. Noble JH, Warren FM, Labadie RF, Dawant BM, “Automatic segmentation of the facial nerve and chorda tympani in CT images using spatially dependent feature values,” Med. Phys, 35:5375–5384, 2008. [PubMed: 19175097]

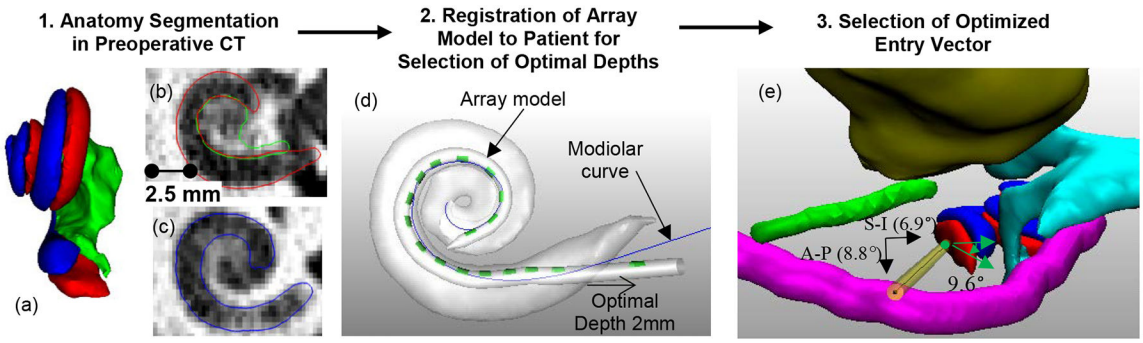

Figure 1:

Shown are the three steps in the proposed image-guided insertion planning process. In (a) are automatically segmented surfaces of the scala tympani (red), scala vestibuli (blue), and modiolus (green). Shown in (b) and (c) are slices in the corresponding pre-operative CT scan with superimposed structure contours. Shown in (d) are the array model (contacts in green) registered to the modiolar curve (blue) of the patient's scala tympani (white), as well as the overall insertion depth recommended based on this registered model. In (e), shown is the view down the control trajectory (green circle) implemented for case #12 relative to the facial nerve (magenta), chorda tympani (green), ossicles (aqua), and external auditory canal (yellow). The optimal trajectory, which is collinear with the basal turn, is shown as the yellow cylinder. The angle of the control trajectory relative to the optimal trajectory is shown for the S-I and A-P directions. The angle between the control and optimal electrode orientation is also shown.

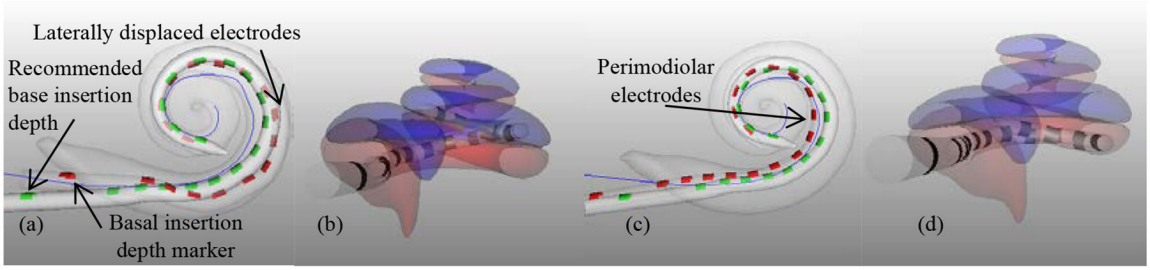

Figure 2.

Shown are the modiolar curve (blue), registered model array (green), and actual final electrode position (red) for case 3 in (a) and 18 in (c) noting that insertion to the generic insertion depth in (a) caused the electrode to become laterally displaced while the electrode in (c) has better perimodiolar position. A lateral-to-medial view of case 3 (b) and 18 (d) show full ST positioning in (d) and a scalar translocation in (b).

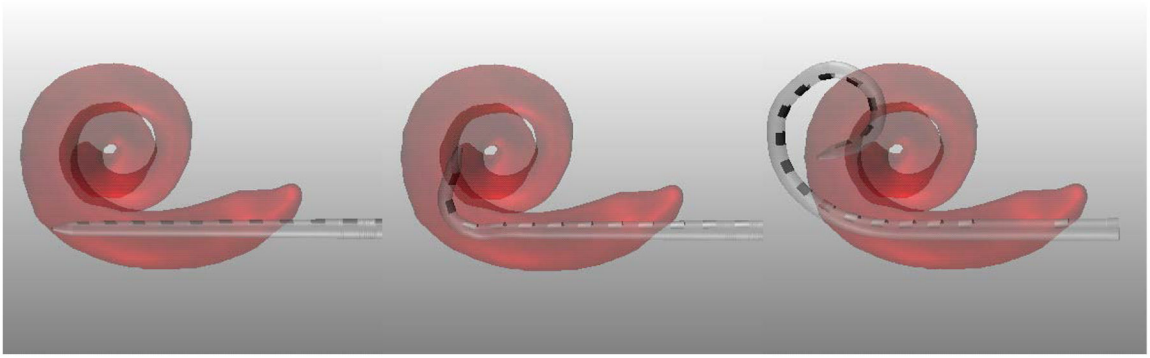

Figure 3.

Shape of the array as it is advanced off the stylet using the control plan AOS and insertion depths for case #12. Shown are the resting state shape of the array when it is advanced 0 mm (a) and 2 mm (b) off the stylet with the stylet at a depth of 7 mm and, in (c), once full insertion depth is reached and the stylet is fully retracted (c).

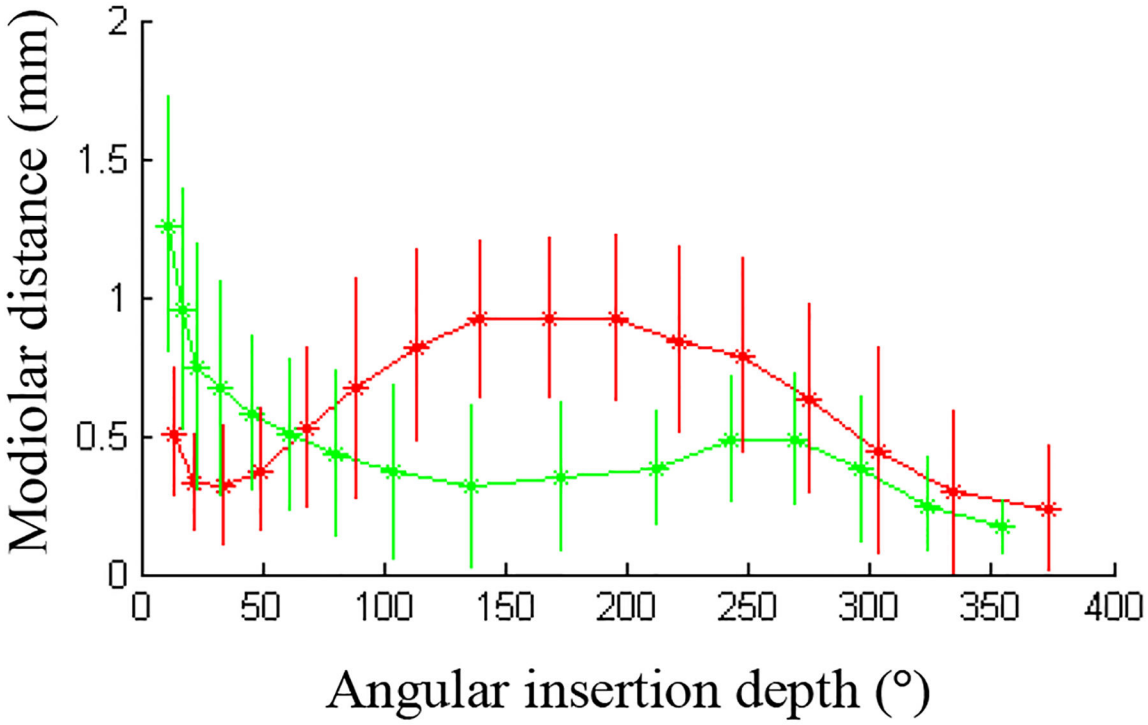

Figure 4.
Average modiolar distance and insertion depth for each electrode in the *A* (green) and *B* (red) groups. Vertical lines indicate standard deviation of modiolar distance.

Table 1.

Experimental Results for Each Case

Case	Group	Scalar Location	Angular Depth (°)	Mean Modiolar Dist (mm)	Actual Overall Depth (mm)	|Actual-Plan Depth| (mm)
1	*B*	ST-SV	276	0.86	−1	1.5
2	*A*	ST	383	0.51	0	0.5
3	*B*	ST-SV	406	0.62	0	0
4	*A*	ST	367	0.41	−2.1	0.1
5	*B*	ST	378	0.61	−1.5	1.5
6	*A*	ST	382	0.49	0	0.5
7	*B*	ST-SV	406	0.75	0	0
8	*A*	ST	356	0.63	−2.6	0.1
9	*B*	ST	375	0.44	−0.8	0.8
10	*A*	ST	359	0.61	−4	1.5
11	*B*	ST	404	0.54	0	0
12	*B*	ST-SV	388	0.75	−0.9	0.9
13	*A*	ST	362	0.43	−2.1	1.1
14	*A*	ST	352	0.61	−2.9	0.4
15	*A*	ST	358	0.48	−2.5	0
16	*B*	ST	373	0.37	−1.4	0.9
17	*A*	ST	327	0.52	−5.4	2.9
18	*A*	ST	375	0.37	−2.8	0.3
19	*B*	ST	383	0.49	−1.3	0.3
20	*B*	ST	372	0.56	−1.2	0.7

Table 2.

Group wise results for proposed and control methods

Value	Group	Scalar Location (ST%)	Angular Depth (°)	Mean Modiolar Dist (mm)	|Actual-Plan Depth| (mm)
Average	*A*	100	362	0.51	0.74
	B	60	376	0.60	0.66
	Pat	47	392	0.54	1.05
St. Dev.	*A*		16	0.09	0.89
	B		38	0.15	0.58
	Pat		75	0.13	0.74
p	*A* vs *B*	**0.030**	0.302	0.115	0.815
	A vs Pat	**0.006**	0.130	0.501	0.368
	B vs Pat	0.543	0.473	0.284	0.145